Experimental and numerical investigation on stainless steel corrugated girders subjected to patch loading

Engineering Structures 334 (2025) 120221

Contents lists available at ScienceDirect

Engineering Structures

journal homepage: www.elsevier.com/locate/engstruct

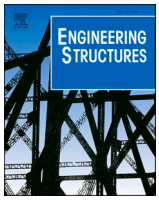

Experimental and numerical investigation on stainless steel corrugated girders subjected to patch loading

Carlos Graciano [a,*], Mathias Flansbjer [b], Mohammad Al-Emrani [c], Mozhdeh Amani [c], Euro Casanova [d]

[a] Universidad Nacional de Colombia, Facultad de Minas Sede Medellín, Departamento de Ingeniería Civil, Medellín A.A 75267, Colombia
[b] RISE Research Institutes of Sweden, Chemistry and Applied Mechanics, Brinellgatan 4, Borås 50462, Sweden
[c] Chalmers University of Technology, Department of Architecture and Civil Engineering, Sven Hultins Gata 6, Gothenburg 41296, Sweden
[d] Universidad del Bío-Bío, Departamento de Ingeniería Civil y Ambiental, Avenida Collao 1202, Concepción, Concepción Código Postal 4051381, Chile

ARTICLE INFO

Keywords:
Stainless steel
Corrugated web girder
Patch loading
Experimental study
Nonlinear finite element analysis
Digital image correlation system

ABSTRACT

This paper presents an experimental and numerical investigation on the structural response of stainless steel trapezoidally corrugated web girders subjected to patch loading. Four girders were tested to failure, the length and position of the patch load within the corrugation profile were varied to investigate its impact on the ultimate load and failure modes. All four girders were made of lean duplex stainless steel (EN 1.4162/LDX 2101). Initial geometric imperfections were measured using a digital image correlation system. The load-displacement responses and the failure modes were analyzed in detail. In addition, geometrically and materially nonlinear analyses with imperfection included (GMNIA) were also performed. Measured initial imperfections were included in the model. The numerical model was verified against the experimental results. Stress distribution plots were also obtained numerically to further analyze the failure modes and the influence of the strain hardening capacity of stainless steel. Ultimate loads obtained experimentally were also compared with predicted resistances using theoretical models available in the literature. According to the results, neglecting the flange resistance to patch loads according to standard EC3:1–5 leads to a significant underestimation of the capacity of stainless steel and carbon steel corrugated web girders. However, considering the resistance from both the flange and web, the difference between the design model and test results is limited to a safe range of 3–12 % for all four tested girders.

1. Introduction

An increasing use of stainless steel in construction has led to the development of several research projects around the world. Particularly, in sustainable construction stainless steel plays an important role in the design of structural components employed in corrosive environments decreasing maintenance costs, and in fire conditions, exhibiting enhanced resistance to high temperatures [1–3]. At present, international standards for the design of stainless steel members [4,5] have been mostly developed aligned with carbon steel design provisions [6,7]. These provisions consider an idealized elastic perfectly plastic material behavior, which is typical for carbon steel. Stainless steel exhibits nonlinear material strain-stress curves with significant strain hardening that should be considered in strength calculations for economical and efficient structural designs [8–10].

Over the last two decades several investigations have been conducted on the resistance of stainless steel plate girders with flat webs subjected to concentrated loads. Unosson et al. [11–13] studied both experimentally and numerically the structural response of patch-loaded stainless steel girders. Dos Santos et al. [14] also investigated experimentally and numerically the resistance to patch loading of welded stainless steel girders with stocky and slender flat web plates. The results of these studies demonstrated conservatism in using the current design models to predict the patch loading resistance of stainless steel plate girders [4,5]. These design models were mostly developed based on research conducted on carbon steel girders neglecting the pronounced strain hardening exhibited by stainless steel. To overcome this situation, Graciano et al. [15], and Dos Santos and Gardner [16] developed numerical databases and proposed calibrations of the resistance model in the European standard for the design of stainless steel members EC3:1–4

* Corresponding author.
E-mail address: cagracianog@unal.edu.co (C. Graciano).

https://doi.org/10.1016/j.engstruct.2025.120221
Received 29 September 2024; Received in revised form 9 February 2025; Accepted 25 March 2025
Available online 10 April 2025

[4]. A significant improvement in the predicted resistance was attained in both works. Using a machine learning approach, Graciano et al. [17] also proposed a formula for the patch loading resistance of stainless steel plate girders. In recent years, the stability of stainless-steel frames has also been investigated [18–21].

In comparison to flat webs, the transversal and vertical stiffnesses of corrugated web girders are larger than those corresponding to flat webs. For patch loaded plate girders, the folded webs enhance out-of-plane stiffness making the web more resistant to buckling and diminishing the need to add vertical stiffeners or to increase the web thickness, which may lead to reduce design costs. Several studies have been conducted on the structural response of carbon steel corrugated web girders subjected to patch loading. Leiva-Aravena and Edlund [22] conducted a set of experiments on plate girders with trapezoidal corrugated webs subjected to patch loading varying the web thickness, loading length, and loading position, namely, above the center of an inclined fold, the center of a longitudinal fold or at an edge between two folds. Kähönen [23] performed tests on corrugated web girders varying the girder geometry and proposed a formula to predict the resistance to patch loading. Using nonlinear finite elements analysis, Luo and Edlund [24] investigated the influence of the corrugation geometry, loading length, and material heterogeneity between flat and edges. It was concluded that the most influential parameters are the loading length and the corrugation angle. Elgaaly and Seshadri [25,26] conducted both experimental and numerical investigations on corrugated web girders subjected to short-length patch loads representing the action between purlins and roof girders. The failure in all tested girders was due to vertical bending of the flange and crippling of the web under the load.

In a continuing effort to study the structural response of carbon steel corrugated web girders, Kövesdi et al. [27] performed a numerical study based on the experiments conducted by Elgaaly and Seshadri [25]. Based on the verified model a parametric study was performed varying the geometric parameters. Two failure mechanisms were observed, local buckling within the loaded fold and global buckling of the whole web. A design proposal was developed for the local buckling mode of failure. This design proposal is the basis to calculate the patch loading resistance of carbon steel corrugated web girders in the European standard FprEN 1993–1–5 [6]. Kövesdi et al. [27] also presented the results of an experimental campaign in which the loaded length and position, the flange thickness and the girder width were varied. These results were also applied to validate their design proposal.

Based on the tests results presented by Kövesdi et al. [27], Kövesdi and Dunai [28] conducted an extensive parametric study to analyze the failure modes, patch loading resistance, and the influence of initial geometric imperfections (shape and size). Ljungström and Karlberg [29] also conducted an experimental campaign to investigate the effect of the loading location on the patch load capacity of trapezoidal corrugated web girders. Al-Emrani et al. [30] conducted a numerical study through nonlinear finite element analysis, and the numerical model was validated using the results obtained in [29]. A parametric study was performed varying the flange and web thicknesses, size of the initial geometric imperfections, and the loading position. Inaam and Upadhyay [31] conducted a numerical study on corrugated web girders under patch loading considering other static forms such as simply supported girders with overhang, continuous girders and cantilever girders. A design model was proposed for the cantilever configuration. Maiorana et al. [32] investigated numerically the effects of patch loading and load eccentricities on flat and corrugated web girders. Both linear and nonlinear analyses were performed to evaluate the variations in slenderness, aspect ratio, loading length, loading width, and size of the corrugation. Kumar et al. [33] performed nonlinear finite element analysis and proposed an artificial neural networks (ANN)-based formulation to predict the patch loading resistance of corrugated web girders having equal or unequal corrugation folds for simply supported and cantilever forms. It was found that the ANN-based formulations achieved more accurate estimations of patch loads compared to other existing models available in the literature. Kumar et al. [34] conducted an extensive literature review on the behavior of corrugated web girders under various loading conditions. Recently, combining the geometric and material assets of corrugated webs and stainless steel respectively, Sæmundsson and Ingólfsdóttir [35] performed a numerical study on the nonlinear structural response of stainless steel corrugated web girders subjected to patch loading. Instead of using trapezoidal profiles, Pasternak and Branka [36] and Nikoomanesh et al. [37] investigated the patch loading capacity of sinusoidal corrugated webs.

As seen in the literature review, the structural response of stainless steel corrugated web girders subjected to patch loading has only been studied numerically [35], and a methodology for the prediction of the resistance to patch loading for these girders is not currently available in the field. Therefore, this paper presents an experimental investigation of the structural response of stainless steel corrugated web girders subjected to patch loading. Four corrugated web girders made of lean duplex stainless steel (EN 1.4162/LDX 2101) are tested to failure. The effects on the response of the loading length and position, and the consideration of unequal fold lengths were investigated. Initial shape imperfections were measured using a digital image correlation (DIC) system. Load-displacement responses and the failure modes were analyzed in detail. In addition, geometrically and materially nonlinear analyses with imperfection included (GMNIA) were also performed. A numerical model was elaborated through nonlinear finite element analysis. Measured initial imperfections were included in the model. A verification of the computational model was performed using the experimental results. Stress distribution plots were also obtained numerically to further analyze the failure modes, and to analyze the influence of the strain hardening capacity of stainless steel. The ultimate loads obtained experimentally were also compared with predicted resistances using theoretical models available in the literature.

2. Experimental setup

2.1. Specimen geometry

Fig. 1 illustrates a schematic view of a simply supported plate girder with corrugated web subject to patch loading. In Fig. 1, the corresponding notation is also presented: F is the applied load, a is the girder length, s_s is the patch load length, h_w is the web depth, t_w is the web thickness, b_f and t_f are the flange width and thickness, respectively.

Fig. 2 shows the geometric parameters used to describe the corrugated web panels, in which a_1 and a_2 are the length of the flat and inclined folds of the corrugation, α is the corrugation angle.

Table 1 shows the nominal dimensions of the tested girders. Four loading cases were analyzed namely: edge (E), parallel (whole - W), parallel fold (P), and inclined fold (I). Fig. 3 depicts the four locations used to apply the load across the entire width of the upper flange. Two patch loading lengths were employed in the study: s_s= 100 mm and s_s= 300 mm. The girders were labelled as follows: SSCWE100 corresponds to a stainless-steel corrugated web (SSCW) with the load applied at the edge (E) between a parallel (P) and an inclined fold (I), and a patch load length s_s= 100 mm.

The nominal depth and thickness of the corrugated webs are h_w= 1400 mm and t_w= 6 mm, respectively (h_w/t_w=233), except for the web plate of SSCWP100, which is cut 100 mm shorter, resulting in a depth of 1300 mm (h_w/t_w=217). The nominal dimensions of the flanges for all tested girders are: width b_f= 250 mm and thickness t_f= 25 mm. In addition to the patch loading length s_s, the projected lengths over the edges of the trapezoidal corrugated web defined as effective loading lengths $s_{s,eff}$, are also presented for all four loading cases in Table 1 (Fig. 3).

Additionally in Table 1, the length of one-half wave $w(= a_1 + a_4)$, and the unfolded length of one half-wave $s(= a_1 + a_2)$ for each girder are reported (Fig. 2). The ratio s/w represents the length of the plate used to produce the corrugated web per unit length along the girder. Hence,

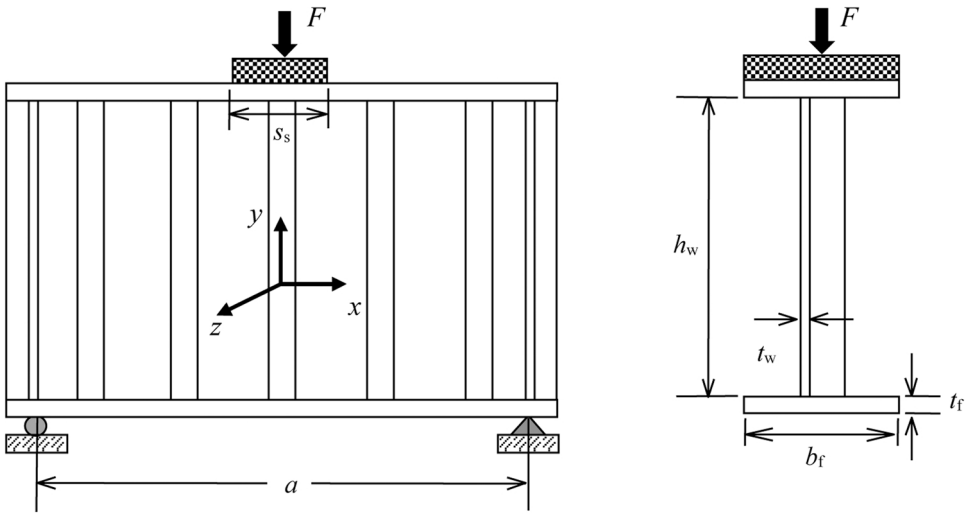

Fig. 1. Corrugated web girder subjected to patch loading (Notation).

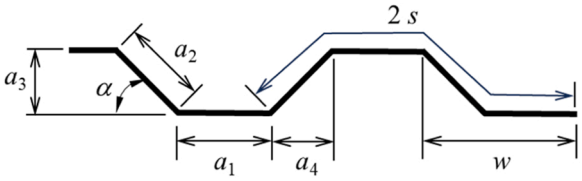

Fig. 2. Geometric parameters of a corrugated web.

higher values of s/w indicate more material consumption in the girder's web for a given web thickness and depth.

Fig. 4 shows a plan view of the upper flanges indicating the location of the patch loads for each tested girder. In addition, the dimensions and configuration of the vertical stiffeners are also reported.

2.2. Boundary conditions and loading protocol

The tests were conducted in a universal testing machine (UTM) with a maximum capacity of 2000 kN, and employing a displacement control routine, the load was applied quasi-statically with a 1.2 mm/min rate. The girders were tested by applying the load at midspan, and the ends

Table 1
Geometry of the corrugation for the tested girders.

Specimen	a (mm)	a_1 (mm)	a_3 (mm)	α (°)	a_2 (mm)	s (mm)	w (mm)	s_s (mm)	s_{s_eff} (mm)	F^{EXP} (kN)
SSCWE100	1538	170	60	35	104.61	274.6	255.7	100	111	1264.0
SSCWW300	1614	170	60	45	84.85	254.8	230.0	300	354	1962.1
SSCWP100	1568	170	100	35	174.34	344.3	312.8	100	100	1206.9
SSCWI100	1624	170	100	45	141.42	311.4	270.0	100	141	1355.7

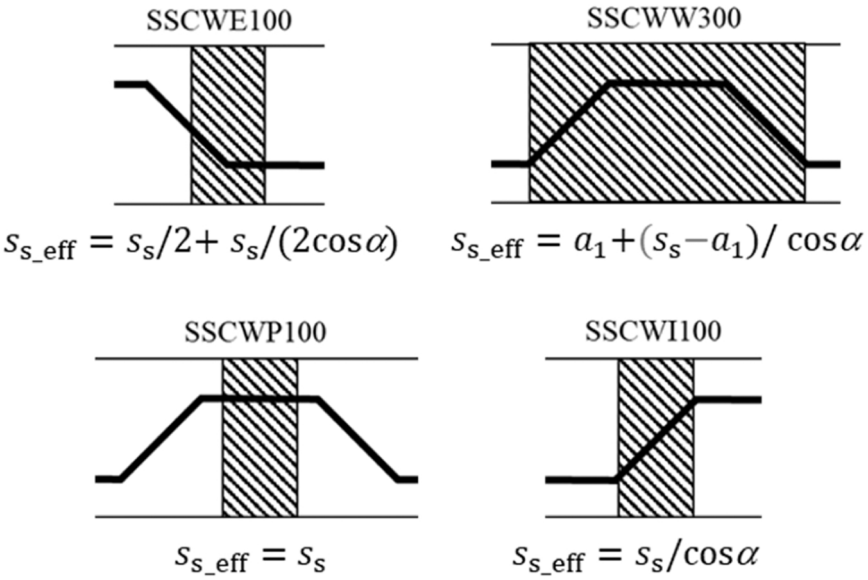

Fig. 3. Loading cases and effective loading lengths s_{s_eff} for girders the tested girders.

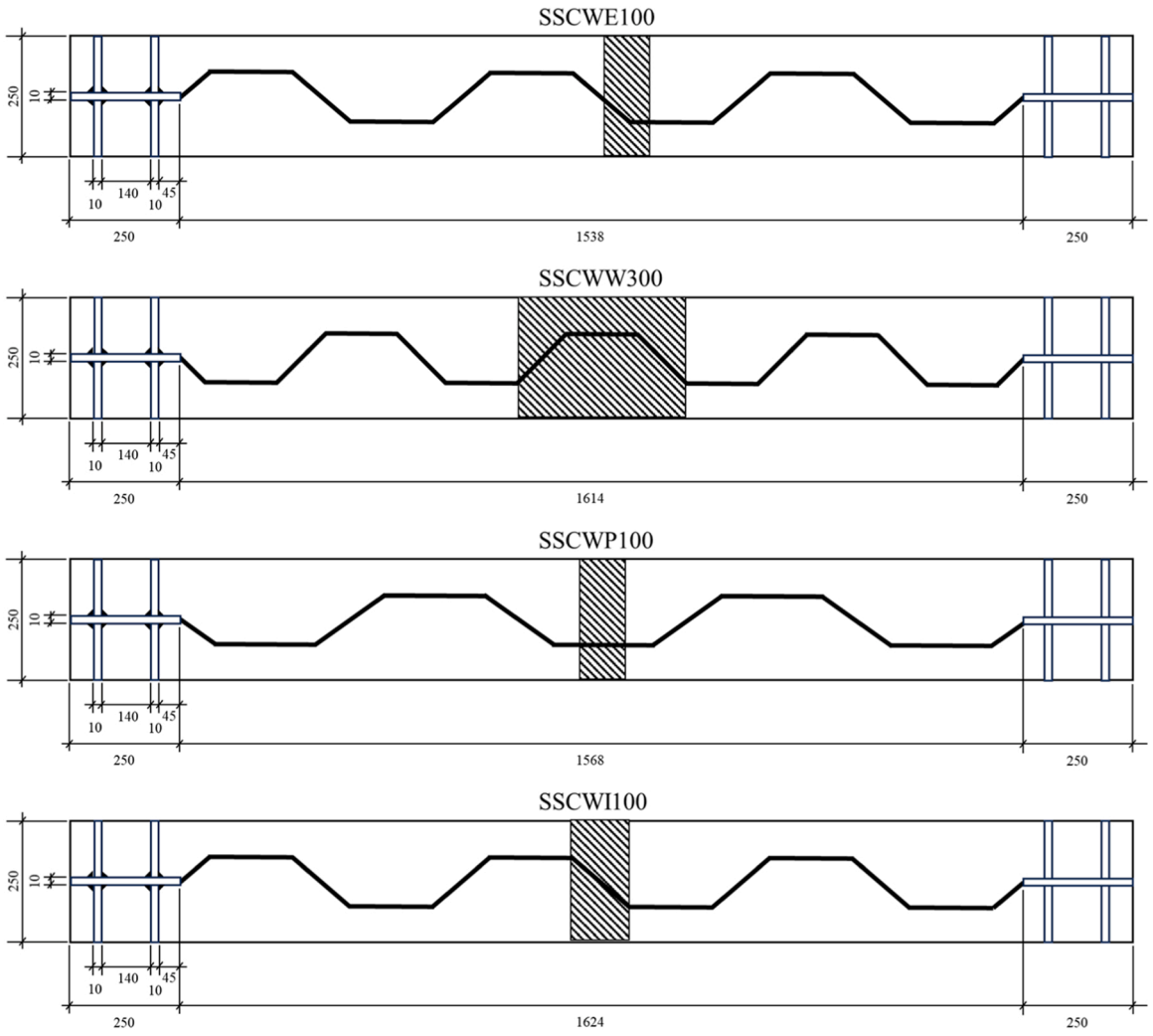

Fig. 4. Plan view of the loaded flanges - Dimensions in mm.

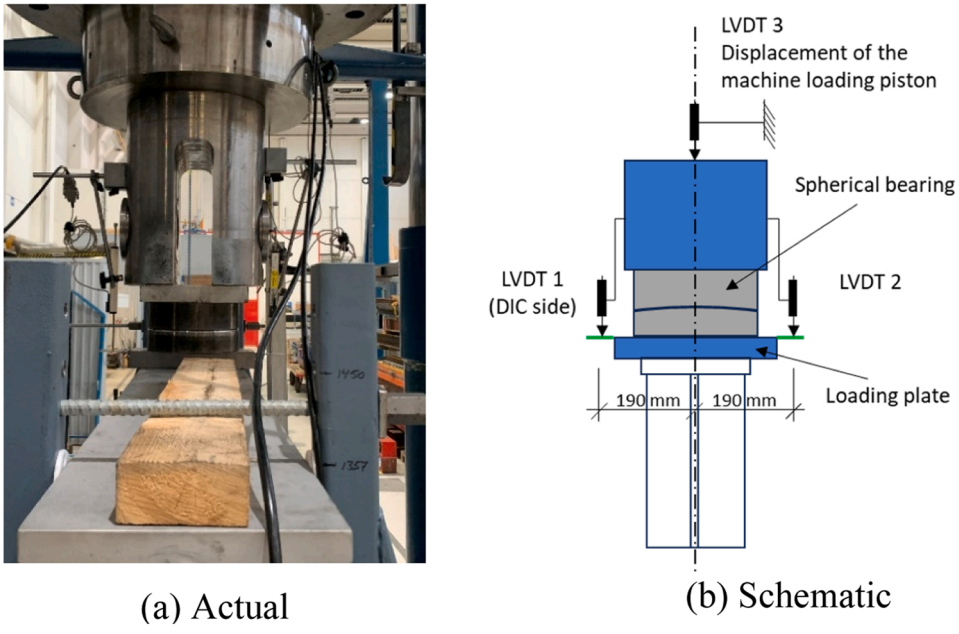

Fig. 5. Setup of LVDTs.

were simply supported. As shown in Fig. 5a, the load is applied through a spherical bearing that is placed on top of a steel plate to distribute the load to the upper flange. The vertical displacements of the girder at the loading point were measured using three linear variable displacement transducers (LVDTs), one measuring the vertical displacement and two measuring possible inclination of the loading plate (Fig. 5b). Load and displacement values were acquired employing a measuring system belonging to the UTM with a frequency of 10 Hz.

Fig. 6a shows the experimental setup for stainless-steel plate girders with corrugated webs subjected to patch loading. Lateral displacements (out-of-plane) at both supports were restricted using fork supports avoiding lateral-torsional buckling (Fig. 6b). Moreover, to avoid the risk of local failure under concentrated forces in the supports, vertical stiffeners were welded at each end. All girders were supported on two rollers placed at each end of the span. The vertical stiffeners at both supports are reinforced with a steel plate (250 × 250 × 20 mm), placed between the roller and the bottom flange (Fig. 4). One of the supports can tilt to compensate for possible small non-straightness of the bottom flange. The supports are also provided with end stops to prevent the girder from rolling off the support at failure. The longitudinal movement is allowed using Teflon sheets between the flange and the fork support.

2.3. Material properties

All four girders were made of lean duplex stainless steel EN 1.4162/LDX 2101. According to the EN ISO 6892–1 Standard [38], a tensile test was conducted on a coupon taken from a parallel fold of the corrugated web plate. From the material curve plotted in Fig. 7, the following material properties were obtained: elastic Young's modulus E= 200 GPa, yield stress is f_y= 550 MPa, and ultimate stress is f_u= 769 MPa. These corrugated web panels came from the same batch employed by Amani et al. [39].

2.4. Initial geometric imperfections and full-field displacement measurements

Initial geometric imperfections and the full-field displacement distribution of the trapezoidal corrugated girder webs were measured using a Digital Image Correlation (DIC) technique. As shown in Fig. 8, the 3D-DIC system was used to measure the out-of-plane displacements of a portion of the web, of approximately 500 × 600 mm, beneath the loading area using the optical system ARAMIS 12 M [40]. Two high-resolution cameras were employed to monitor the displacements in the delimited region of the web during the tests. A random speckle pattern was also delimited in this area employing white retro-reflective

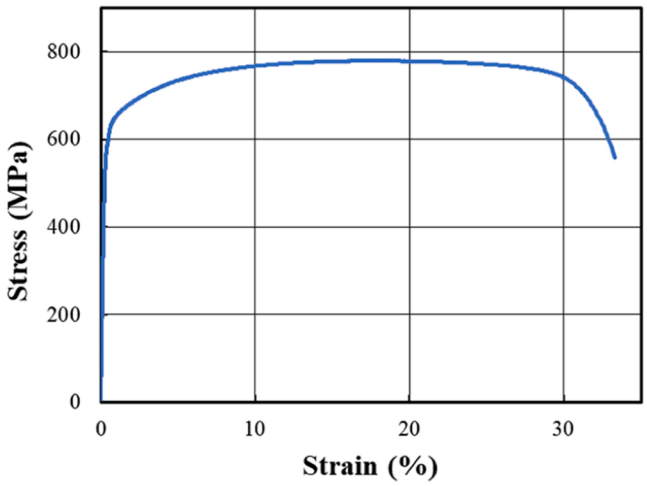

Fig. 7. Engineering stress-strain curve for EN 1.4162/LDX 2101 lean duplex stainless steel.

paint as a background on the web panel, then applying black stains using a rough plastic brush. The ARAMIS system [40] enables real-time tracking and visualization of the displacement values on the delimited surface of the specimens. It creates a series of spatial data points, which are mapped to create the displacement field. Before loading the girders, the DIC system was used to scan the spatial data points making it possible to build the initial geometry of the web panel in the area indicated in Fig. 8. The load and displacement from the testing machine were simultaneously recorded in the DIC system.

The full-field displacement measurements of the initial geometric imperfections of the tested girders web were obtained after digital processing and interpolation of the data. These initial geometric imperfections are displayed in Fig. 9. Table 2 presents the maximum and minimum imperfection amplitudes measured for each tested girder web. In the literature, the magnitude of the initial geometric imperfections w_o for plate girders is limited to $w_o \leq h_w/200$ [6], and for corrugated web girders limited to $w_o \leq a_i/200$ [27], where $a_i = \max(a_1, a_2)$. For girders SSCWE100, SSCWW300, and SSCWI100 the initial geometric imperfections are within the range $w_o \leq$ mm ($w_o \leq h_w/200$). This value is slightly exceeded for girder SSCWP100 ($w_o \leq h_w/196$). In all cases, the magnitude of the imperfections is larger than the recommended values for corrugated web girders $w_o \leq a_i/33$.

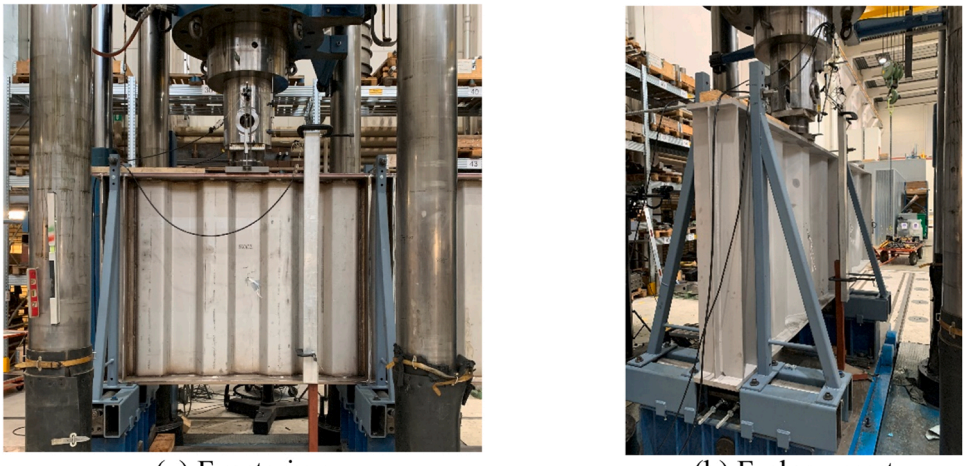

Fig. 6. Experimental setup (Girder SSCWW300).

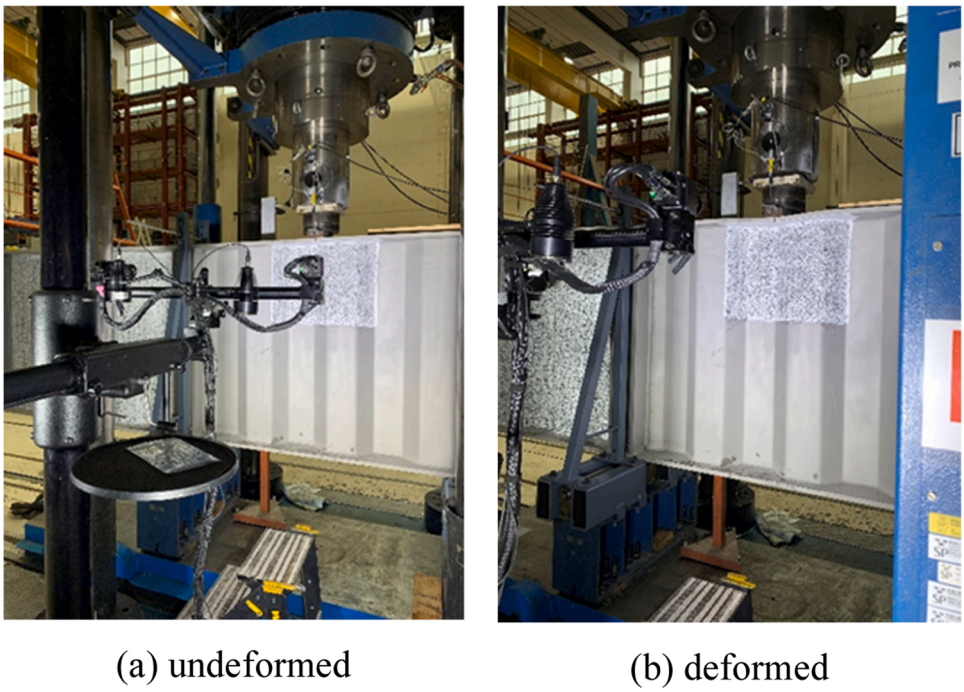

Fig. 8. DIC system setup for specimen SSCWI100.

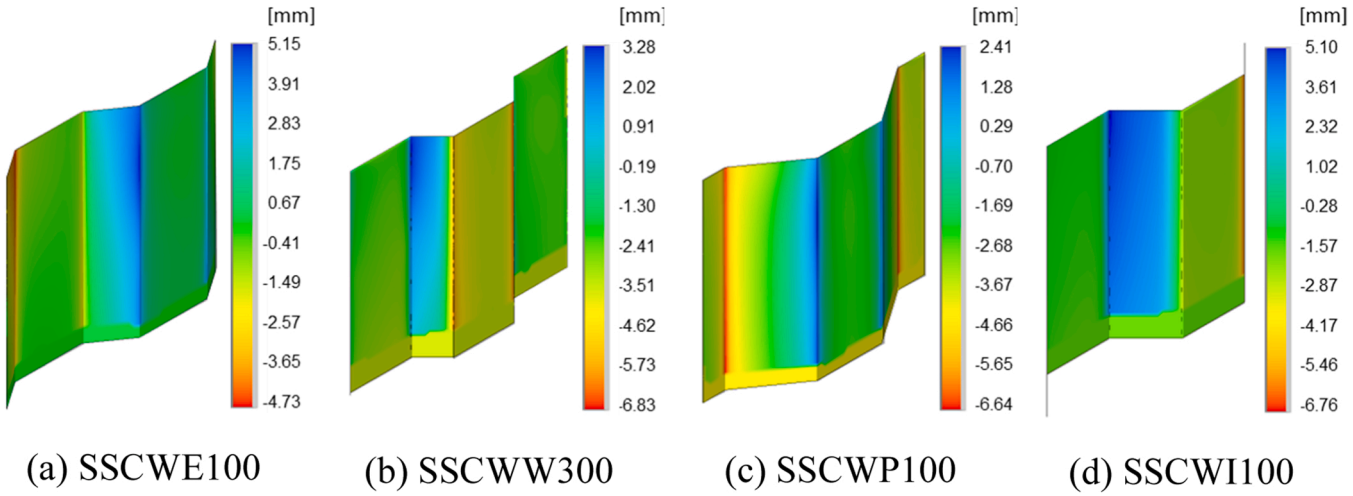

Fig. 9. Measured initial geometric imperfections for the tested girders.

Table 2
Maximum and minimum measured web imperfection amplitudes.

Girder	w_0 (mm)		Ratio
	Max.	Min.	
SSCWE100	+ 5.15	−4.73	$h_w/272$ ($a_i/33$)
SSCWW300	+ 3.28	−6.83	$h_w/205$ ($a_i/25$)
SSCWP100	+ 2.41	−6.64	$h_w/196$ ($a_i/26$)
SSCWI100	+ 5.10	−6.76	$h_w/207$ ($a_i/21$)

3. Test results and discussion

3.1. Load-displacement responses

Fig. 10 shows the load-displacement responses recorded for the tested girders. The experimentally measured ultimate loads F^{EXP} for each

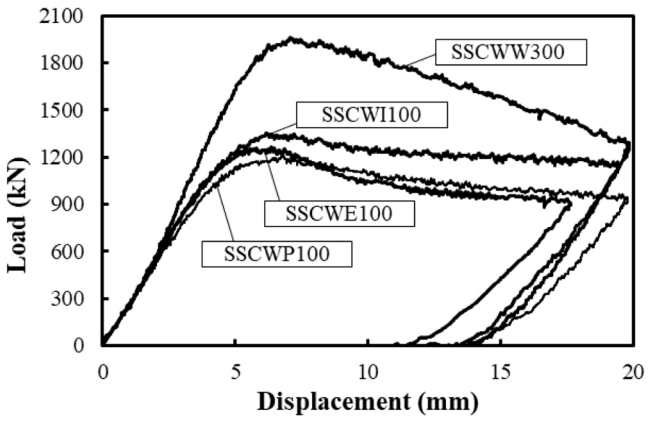

Fig. 10. Load-displacement responses for the tested girders.

girder are also reported in Table 1. As shown in Fig. 4, the load was applied at four different locations. At first glance, it seems that the effect of the location within the corrugation profile is minimal, but on closer scrutiny, it affects the effective loading length s_{s_eff}. Moreover, it is observed that the ultimate load of the girders increases with the loading length s_s (Fig. 10). For girders SSCWE100, SSCWP100, and SSCWI100 with short loading length s_s= 100 mm and different loading locations, the magnitudes of the ultimate loads were similar, for girder SSCWE100 with the load applied over an edge the ultimate load was F^{EXP}= 1264.0 kN, for girder SSCWP100 with the load applied within a parallel fold the ultimate load was F^{EXP}= 1206.9 kN, and for girder SSCWI100 with the load applied over an inclined fold the ultimate load is slightly higher F^{EXP}= 1355.7 kN. Girder SSCWW300 with a longer loading length (s_s=300 mm in Table 1) achieved the highest ultimate load F^{EXP}= 1962.1 kN.

As shown in Fig. 3, the effective loaded length s_{s_eff} in corrugated web panels is larger than the loading length s_s measured parallel to the loaded flange. For girder SSCWE100 s_{s_eff}= 111 mm, for SSCWW300 s_{s_eff}= 354 mm, for SSCWP100 s_{s_eff}= 100 mm, and for SSCWI100 s_{s_eff}= 141 mm. Fig. 11 shows that there is a linear relationship between the ultimate loads and the effective loaded lengths for stainless steel corrugated web panels. The effective loading length considers both the fold dimensions and the corrugation angle.

3.2. Failure modes

Fig. 12 shows the failure modes of the tested girders. In all cases, the girders failed due to local web buckling within the folds located beneath the loading plate. For girders SSCWE100 (Fig. 12a), SSCWP100 (Fig. 12c), and SSCWI100 (Fig. 12d), the failure is very localized in the fold beneath the loading area. In these three cases the buckle is limited by the fold lines. For girder SSCWW300 (Fig. 12b), the directly loaded folds buckle simultaneously, and then it spreads over the two adjacent folds after the fold lines fail. Similar results were reported by Kövesdi et al. [27] for carbon steel corrugated web girders with equal fold lengths ($a_1 = a_2$).

Kumar et al. [33] demonstrated that for corrugated web girders the fold length ratio a_2/a_1 affect the patch loading resistance, reaching a maximum value when the ratio was within the range $0.50 \leq a_2/a_1 \leq 0.75$, irrespective of the variation of the geometric parameters or type of static form (simply supported or cantilever). For lower ratios a_2/a_1 the unsupported flange outstands increase, and for higher ratios the span of the local flange beam, defined as the cantilever from vertical web plane and a beam longitudinally supported between inclined folds) increase.

For girders SSCWE100, SSCWP100, and SSCWI100 with the same loading length s_s= 100 mm the fold length ratios a_2/a_1 were 0.62 (F^{EXP}=1264.0 kN), 1.03 (F^{EXP}=1206.9 kN), and 0.83 (F^{EXP}=1355.7 kN) respectively. The lowest ultimate load was achieved for girder SSCWP100 with a fold length ratio $a_2/a_1 \geq 1$, and the highest was achieved for girder SSCWI100 with a fold length ratio a_2/a_1 = 0.83. The fold length ratio for girder SSCWI100 lies outside the optimum range defined in [33], but the load was applied over an inclined fold with equal flange outstands. It gives a clear indication that there is a relationship between the location of load, the flange outstand, and the ultimate load Further studies are necessary to establish this relationship.

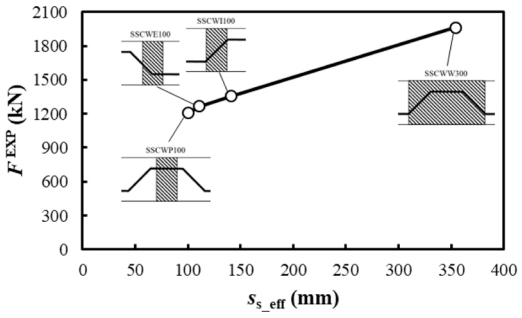

Fig. 11. Experimental ultimate loads F^{EXP} versus effective loading length s_{s_eff} in the web panel.

Nowadays, strict quality control in the manufacturing process of steel components, accompanied by accurate measuring systems for strains and displacements allow researchers to conduct experimental tests with a reduced number of samples. Despite that only four tests were conducted herein, the results presented in this section show consistency with results previously reported in the literature for corrugated web girders subjected to patch loading.

4. Numerical modelling

4.1. GMNIA

In this section, a geometrically and materially nonlinear analysis with imperfections included (GMNIA) is performed. A numerical model was elaborated through nonlinear finite element analysis using the software ANSYS [41]. Shell181 elements were employed to model the flanges, vertical stiffeners, and the trapezoidal corrugated webs. The load was applied through a thick plate over a loading length s_s. The plate thickness is 3 times the flange thickness (i.e. 75 mm) and was modeled with Solid185 3D elements. The contact between the plate and the top flange was modeled with Target170 and Contact174 elements using the Augmented Lagrangian algorithm with a friction factor of 0.3. The arc-length method was used to trace the nonlinear path in the response. The boundary conditions were similar to those employed in the experiments, *i.e.* simply supported conditions and lateral supports at the ends. As shown in Fig. 13, two boundary conditions were applied to the model, first, for the support ends, simple support conditions are defined, i.e. displacements in X, Y and Z directions were restricted in the nodes along support A ($U_X = U_Y = U_Z = 0$), and the nodes on support B were free to move longitudinally ($U_Y = U_Z = 0$).

The measured initial shape imperfections attained with the DIC system were also included in the computational model. The DIC measured real geometry portion of the webs plate were exported in STL format files. From these data, the *z*-coordinate for each node in this portion of the mesh was interpolated creating a surface. This surface overlapped with the perfect geometry of the corrugated web plate.

The engineering stress-strain curve plotted in Fig. 7 is converted into true stress-strain values as defined in prEN 1993–1–14 [42] and introduced to the numerical model. Moreover, the elastic Young's modulus and Poisson's ratio are assumed to be 200 GPa and 0.3, respectively. A multilinear isotropic hardening material model with a von Mises yield criterion was employed. Residual stresses due to cold forming operations during the manufacturing process of corrugated plates may affect the material properties. Nevertheless, previous works on carbon steel [24,27–30] and stainless steel [39] corrugated plate girder webs have demonstrated that strain hardening effects in the edges (bent area) have a negligible effect on ultimate strength.

The numerical model was verified using the results obtained in the experimental campaign. A mesh sensitivity analysis was performed, and shell elements of 10 mm size ($h_w/140 - h_w/130$) were chosen in the final meshes (Fig. 13). This element size is smaller than those used in most of the previous works modelling corrugated girders, as reported by Kumar et al. [34]. A final mesh with 57069, 59265, 58170, and 60901 elements was chosen for girders SSCWE100, SSCWW300, SSCWP100 and SSCWI100, respectively.

4.2. Comparison of load-displacement responses and resistances

Fig. 14 shows a comparison between the load-displacement responses obtained experimentally and numerically for the tested girders.

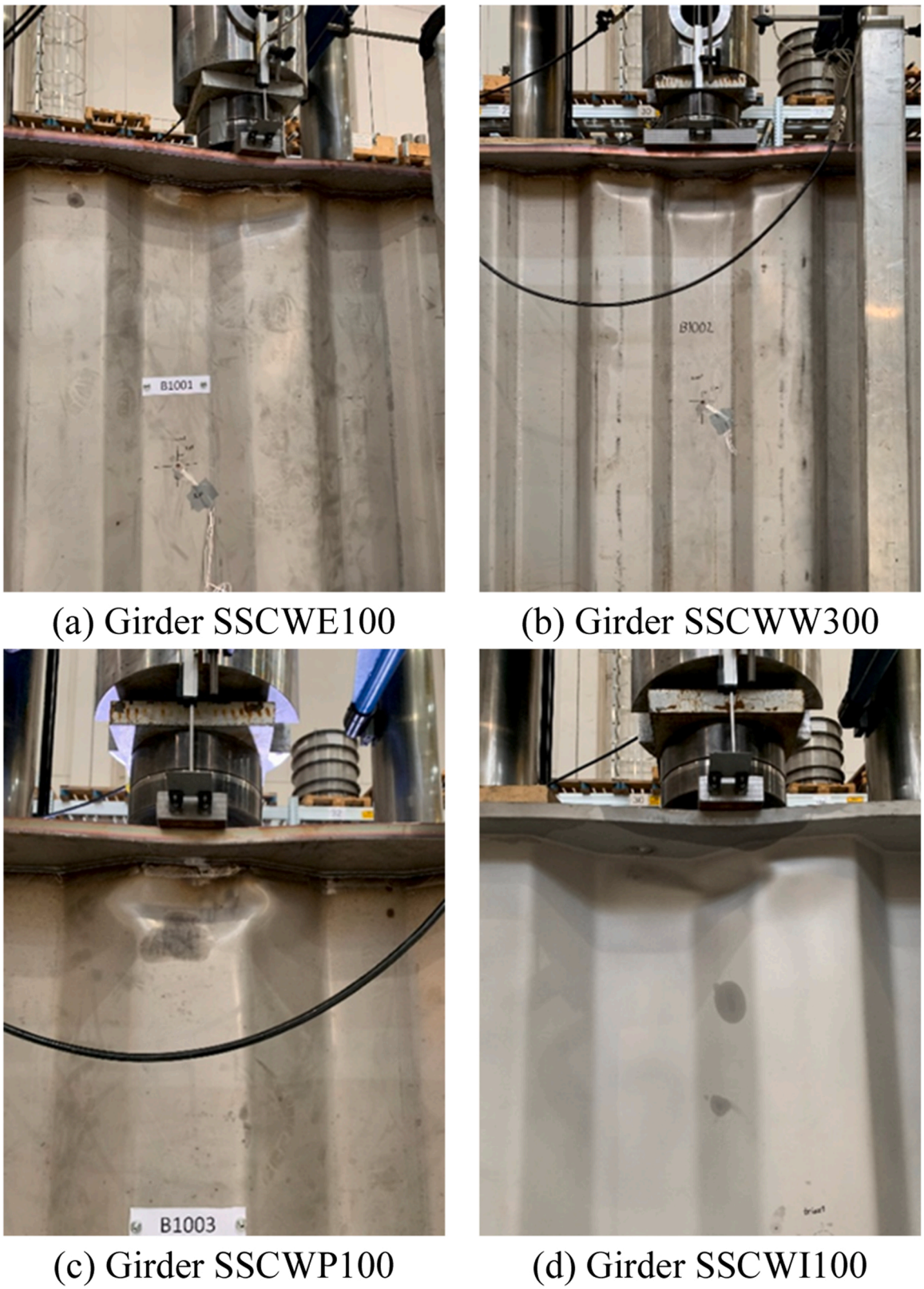

Fig. 12. Failure modes of the tested girders.

In Fig. 14a, the numerical response of girder SSCWE100 follows the test load-displacement curve, and both experimental and computed ultimate loads are comparable. The ultimate loads are 1264.0 kN and 1318.4 kN for the test and the numerical model, respectively, with a difference of 4.3 %. The postbuckling response obtained numerically is different than the test results. Fig. 14b presents the load-displacement curve for girder SSCWW300, which shows an enhanced ultimate load compared to SSCWE100 due to an increased loading length. The initial slopes of the load-displacement curves from the test and the model are very close, after certain load the slope of the numerical curve is slightly steeper, and

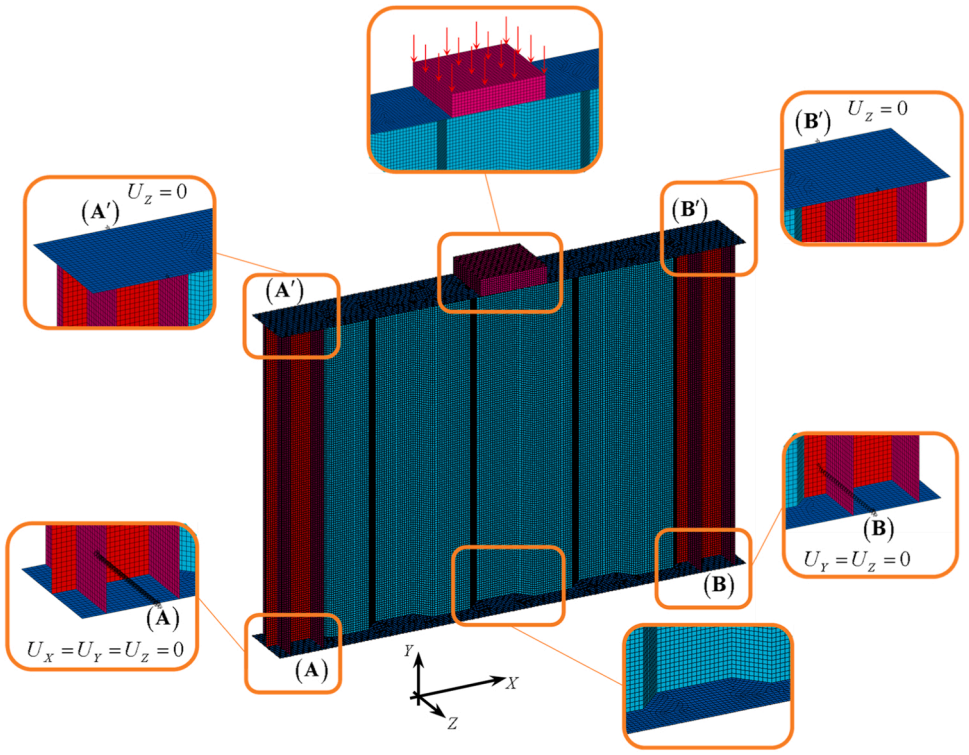

Fig. 13. Numerical model-final mesh (Girder SSCWW300).

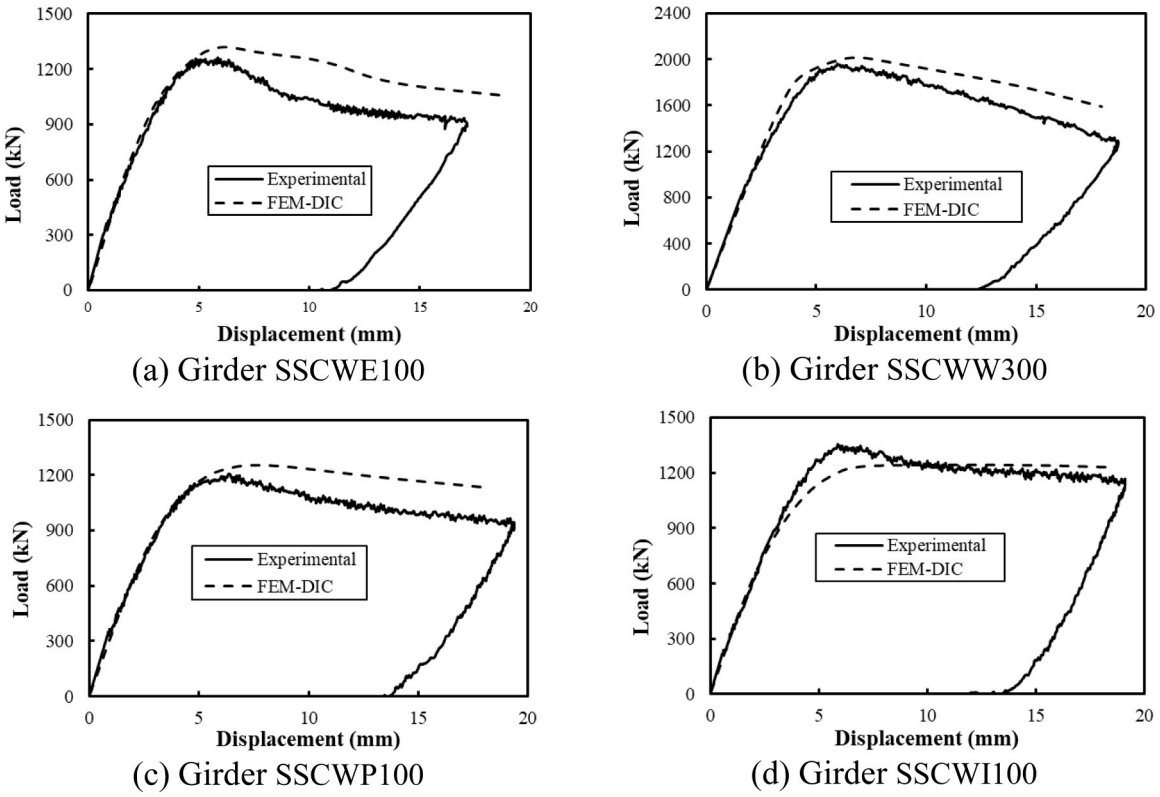

Fig. 14. Comparison between experimental and numerical load-displacement responses.

its deflection is smaller compared to the test data. However, as the load increases the slope of the experimental curve gradually decreases in comparison to the numerical response, achieving the ultimate load at 1962.1 kN for the test and 2013.6 kN for the model, that represents a difference of 2.6 %.

Fig. 14c compares the test and numerical load-displacement curves for girder SSCWP100, both curves exhibit identical initial stiffnesses, and the ultimate loads are quite close, 1206.9 kN in the test and

1253.3 kN in the simulation, representing a difference of 3.8 %. Finally, Fig. 14d shows the test and numerical responses for girder SSCWI100. For this case, the initial slopes are identical, then the numerical model predicts a lower ultimate load of 1243.1 kN in comparison of 1355.7 kN obtained in the experiments.

Table 3 summarizes the patch loading resistances computed numerically and the test results. Ultimate loads predicted using FEM closely match the experimental results, confirming the model accuracy.

4.3. Displacement and stress distribution plots

Fig. 15 shows the maximum displacements at ultimate load level for the girders considering the experimentally measured initial geometric imperfections. The deformed patterns are similar to those depicted in Fig. 12. Fig. 16 shows the von Mises stress distribution plots at the ultimate load level for the girders considering the experimentally measured initial shape imperfections. In all cases the maximum stresses are achieved in the zone beneath the loading area. The level of these stresses over large areas beneath the load are between the yield strength (f_y=550 MPa) and the ultimate strength (f_u=779 MPa) for EN 1.4162/LDX 2101 lean duplex stainless steel. It is a clear indication that stainless steel corrugated web girders make use of the enhanced strain hardening capacity of the material.

4.4. Out-of-plane deformation pattern

Regarding the use of experimental instrumentation, it is advantageous to use a DIC system to measure the deformations and displacements on the loaded area as reported in Section 2.4. Fig. 17 shows a comparison between the deformation patterns, and out-of-plane displacements at the end of the loading, measured with the DIC system and those obtained numerically. In all cases, a good correlation for the buckling shapes can be observed between both results.

Fig. 18 presents diagrams for the applied load in terms of the maximum out-of-plane displacement for all the tested girders. These displacements obtained with the DIC system are compared with similar plots obtained numerically. In Fig. 18a, the numerical response for girder SSCWE100 exhibits a stiffer response than in the experimental curve. As seen in Table 2 this girder has the lowest initial geometric imperfection ($w_0 = h_w/272$), the numerical model seems to be unable to reproduce the out-of-plane response of the web. For girder SSCWW300, the numerical model can follow the experimental response sufficiently. As seen in Fig. 18c, the best agreement between experimental and numerical results is attained for girder SSCWP100 when load was applied in a parallel fold. For girder SSCWI100 in Fig. 18d, the numerical model follows the experimental curve at the beginning but predicts a lower resistance.

5. Evaluation of available resistance models

5.1. Patch loading resistance of carbon steel trapezoidal corrugated webs

In the studies conducted by Kövesdi et al. [27] and Kövesdi and Dunai [28], two failure modes were identified depending on geometric parameters. For small local fold ratios (a_i/t_w) and high global web ratios

Table 3
Comparison between patch loading resistances computed numerically F^{NUM} with the test results F^{EXP}.

Girder	F^{EXP} (kN)	F^{NUM} (kN)	Δ [%]
SSCWE100	1264.0	1318.4	−4.3
SSCWW300	1962.1	2013.6	−2.6
SSCWP100	1206.9	1253.3	−3.8
SSCWI100	1355.7	1243.1	8.3

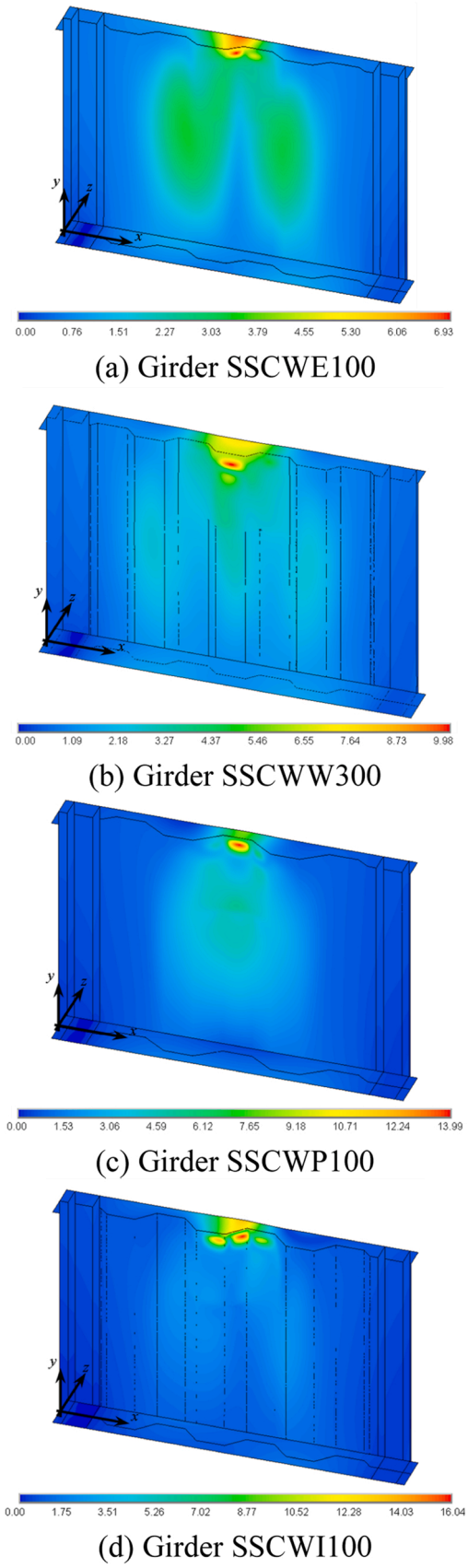

Fig. 15. Displacements plots in (mm) for the girders at ultimate load level considering the measured initial geometric imperfections.

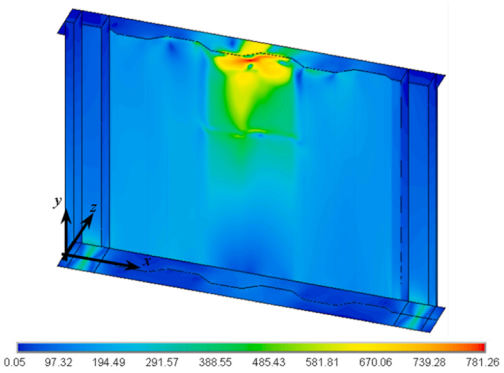

(a) Girder SSCWE100

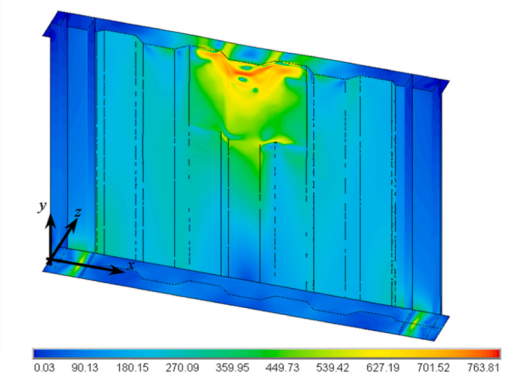

(b) Girder SSCWW300

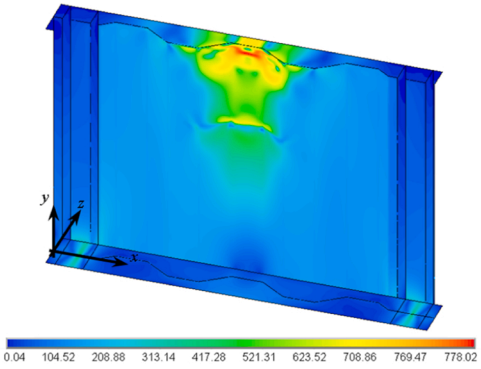

(c) Girder SSCWP100

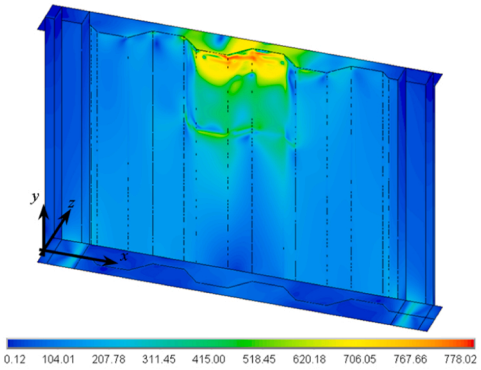

(d) Girder SSCWI100

Fig. 16. Equivalent von Mises stress distribution plots in (MPa) for the girders at ultimate load level considering the measured initial geometric imperfections.

(h_w/t_w=100–200) the failure mode was characterized by global buckling of the whole web under the patch load, and for high local fold ratios the failure mode was characterized by local buckling within the fold. Results from the numerical investigation also showed that the failure mode in the parameter range of bridges is mainly local buckling. Then a theoretical model for local buckling (web crippling) was proposed. This model, based on a four-plastic hinge failure mechanism originally proposed by Rockey and Roberts [43], divides the patch loading resistance F_u into two parts, as follows

$$F_u = 2\sqrt{4M_{plf}t_w\chi f_{yw}} + \chi t_w f_{yw} s_s k_\alpha \tag{1}$$

The first term in Eq. (1) represents the flange contribution, and the second term is the web contribution. In Eq. (1), $M_{plf}(=f_{yf}b_f t_f^2/4)$ is the plastic moment of the flange, χ is a reduction factor due to local buckling, f_{yw} and f_{yf} are the yields stresses of flange and web, respectively, and k_α is the modification factor due to the corrugation angle

$$k_\alpha = \frac{a_1 + a_2}{a_1 + a_4} \tag{2}$$

In the newest draft of the European standard for the design of steel structures prEC3:1–5 [6], the calculation model to determine the design resistance F_R of trapezoidally corrugated webs to local buckling under transverse force (patch loading) is based on Eq. (1). This resistance model neglects the contribution of the flange. Accordingly, the patch loading resistance F_R is expressed as

$$F_R = \frac{\chi \; t_w \; f_{yw} \; s_s \; k_\alpha}{1.20 \; \gamma_{M1}} \tag{3}$$

where γ_{M1} is the partial safety factor, and χ is a reduction factor due to local buckling given by

$$\chi = \begin{cases} 1.0 \text{if} \bar{\lambda}_p \le 1.27 \\ \frac{1.9}{\bar{\lambda}_p} - \frac{0.8}{\bar{\lambda}_p^2} \text{if} \bar{\lambda}_p > 1.27 \end{cases} \tag{4}$$

The slenderness $\bar{\lambda}_p$ parameter is

$$\bar{\lambda}_p = \sqrt{\frac{f_{yw}}{\sigma_{cr}}} \tag{5}$$

and the critical stress σ_{cr} is expressed as

$$\sigma_{cr} = \frac{k_\sigma \; \pi^2}{12(1-v^2)} \quad E\left(\frac{t_w}{a_i}\right)^2 \tag{6}$$

where the buckling coefficient is k_σ= 1.1, and a_i is the loaded fold length. If more folds are loaded, the maximum fold length (a_1 or a_2) should be taken. To ensure local buckling (i.e. prevent global buckling failure), the loaded fold length a_i is limited to

$$a_i \ge \left(\frac{h_w}{t_w} + 260\right)\frac{t_w}{11.5} \tag{7}$$

Eq. (7) is valid for corrugation angles $\alpha > 15°$.

5.2. Comparison between test results and theoretical predictions

At present, theoretical models for the patch loading resistance of stainless steel corrugated web girders are unavailable in literature. The theoretical models described in the Section 5.1 were developed considering an idealized elastic perfectly plastic material behavior, which is typical for carbon steel. Moreover, prediction models defined by Eqs. (1) and (3) are restricted by geometric limits as indicated in Eq. (7). Despite these limitations, this section analyzes the suitability of these models for stainless steel corrugated web girders. Theoretical predictions were calculated using a nominal yield stress value of

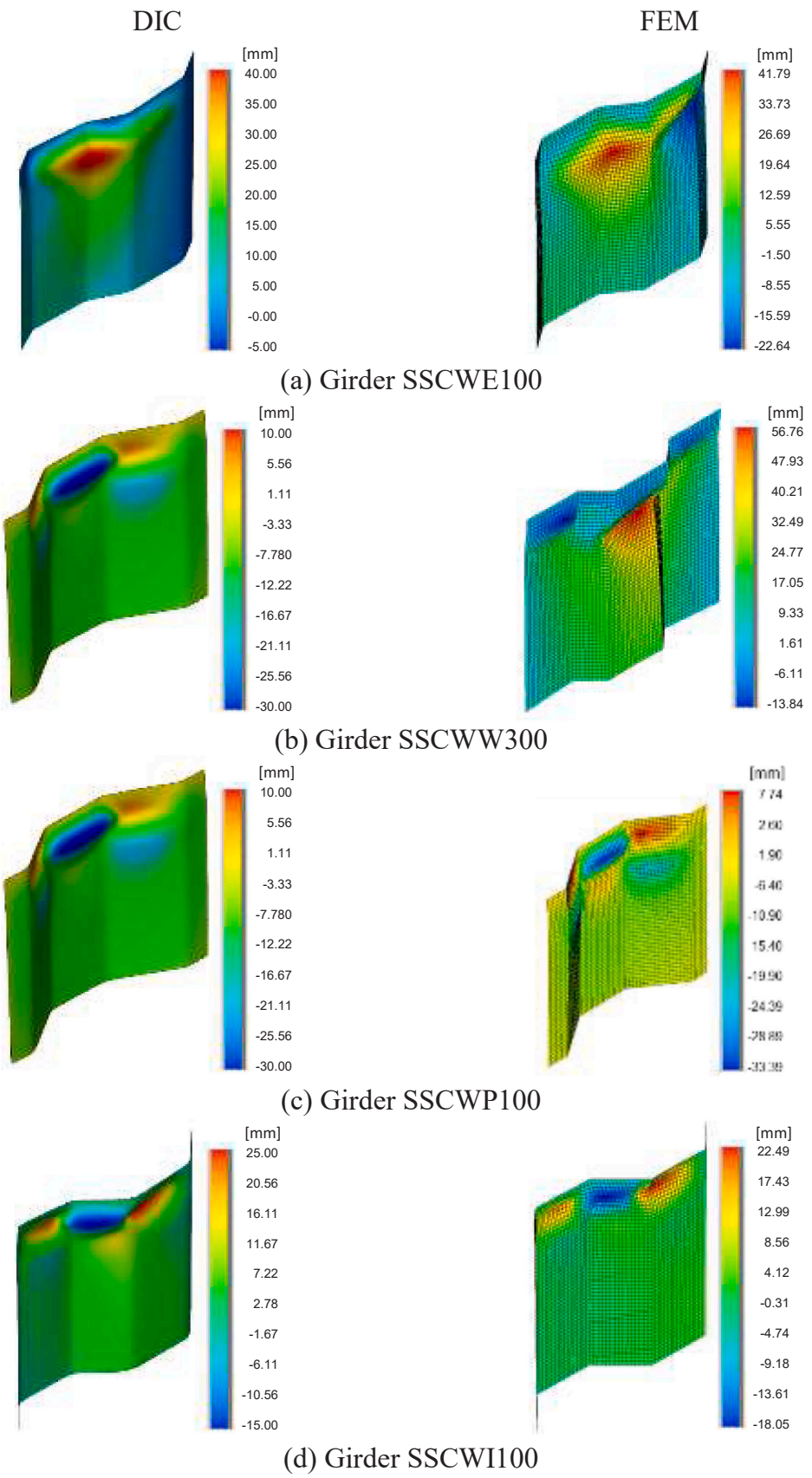

Fig. 17. Comparison between experimental (DIC) and numerical (FEM) out-of-plane displacements (U_z) in the area below the patch load at the end of loading.

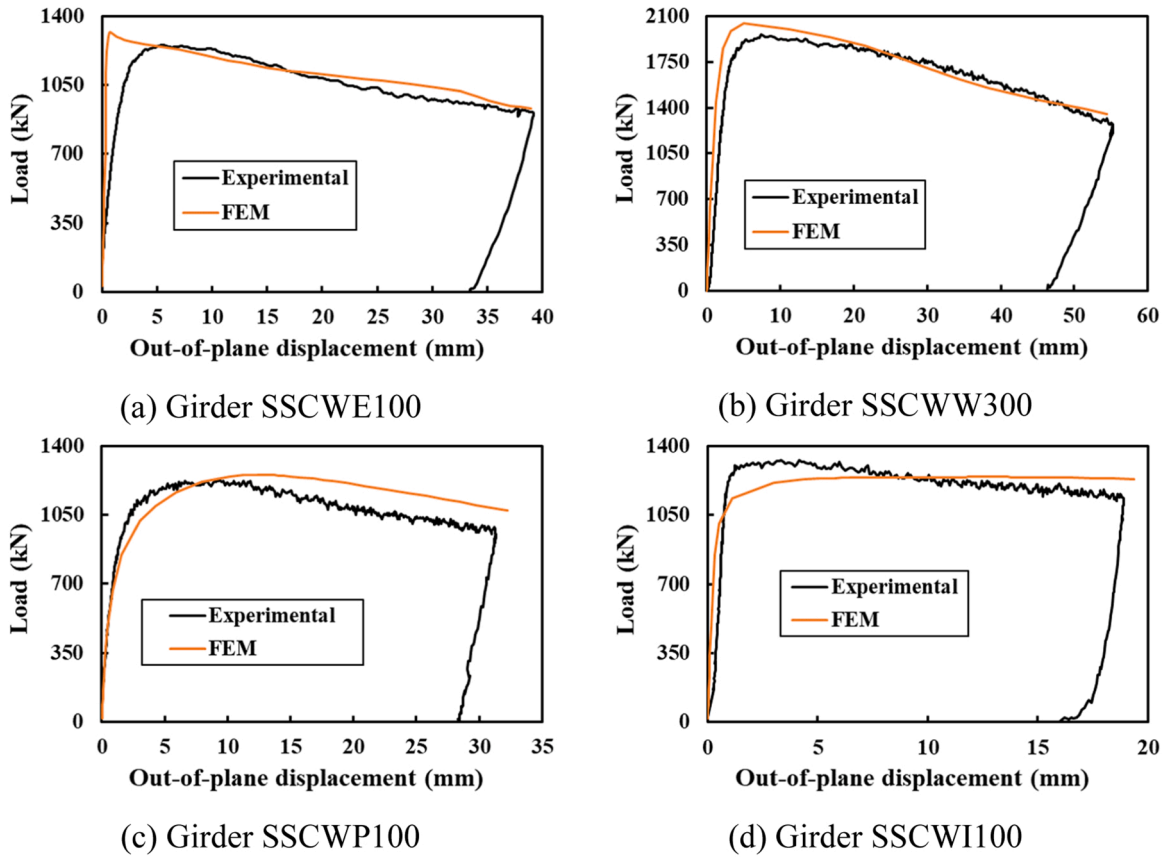

Fig. 18. Comparison between experimental and numerical out-of-plane displacement (absolute values U_z) for the major local buckle in the area below the patch load.

f_y = 460 MPa for EN 1.4162/LDX 2101 lean duplex stainless steel.

According to Eq. (7) and using the dimensions of the tested girders reported in Table 1, to ensure local buckling, the fold lengths for girders SSCWE100, SSCWW300 and SSCWI100 are limited to $a_i \geq 257.4$ mm, and for girder SSCWP100 is limited to $a_i \geq 248.7$ mm. As seen in Table 1, the corresponding fold lengths used herein are smaller than these limit values, however the failure mode of all girders was local buckling as shown in Section 3.2. Table 4 presents a comparison between experimental ultimate loads and predicted patch loading resistances calculated using Eqs. (1) and (3). As mentioned above, Eq. (1) considers the contribution of flange and web. Table 4 also reports the individual contribution of the flange (F_R^{fl}) calculated using the first part of Eq. (1). Predicted resistances using Eq. (1) are close to the experimental ultimate loads, for girder SSCWP100 the difference between these loads is only 3 %, and for girder SSCWI100 the difference is 12 %. In the experiments the size of the flanges was constant, therefore its contribution to the resistance is basically the same for all tested girders. Despite Eq. (1) being developed for carbon steel corrugated web girders and the noncompliance of Eq. (7), the predictions for stainless steel corrugated web girders are very satisfactory.

To quantify the contributions of the webs to the patch loading resistance, the predictions obtained with Eq. (3) considering $\gamma_{M1} = 1$ are reported in Table 4. The corresponding resistances predicted using Eq. (3) are approximately 2.2–4.5 times lower than the test loads, demonstrating conservatism when the contribution of the flanges is neglected in the failure mechanism solution proposed in Eq. (1).

5.3. Comparison with carbon steel girders

In this section, the experimental results for stainless steel (SS) corrugated web girders are compared to those obtained for carbon steel (CS) corrugated web girders. Table 5 summarizes the geometry, material properties, loading conditions, and ultimate loads for the girders tested by Leiva-Aravena and Edlund [22], Elgaaly and Seshadri [26], Kövesdi et al. [27] and Ljungström and Karlberg [29]. In each set of experiments the size of the corrugation was kept constant throughout the tests, Table 6 shows the dimensions of the corrugated profiles.

Fig. 19 presents the experimental ultimate loads F^{EXP} for carbon steel (CS) and stainless steel (SS) corrugated web girders in terms of various geometric parameters. In Fig. 19a, it is clearly observed that the ultimate loads increase with the loading length s_s for carbon and stainless steel girders. As stated by Kövesdi et al. [27], the increase is due to the activation of larger portions of the web in the case of long loading lengths. In Fig. 19b, it seems that the global web ratio (h_w/t_w) has no influence within the range evaluated in the experiments. Nevertheless, in Table 5, a closer look at the results reported by Aravena and Edlund

Table 4
Comparison between the test results and predicted patch loading resistances.

Girder	σ_{cr} (MPa)	$\bar{\lambda}_p$	χ	k_α	$F_u^{Eq.(1)}$ (kN)	F_R^{fl} (kN)	$F_R^{Eq.(3)}$ (kN)	F^{EXP} (kN)
SSCWE100	249.9	1.35	0.96	1.07	1161.8	875.5	286.3	1264.0
SSCWW300	249.9	1.35	0.96	1.11	1761.6	875.5	886.1	1962.1
SSCWP100	249.9	1.35	0.96	1.10	1169.0	875.5	293.5	1206.9
SSCWI100	361.17	1.13	1.00	1.15	1209.1	890.8	318.3	1355.7

Table 5
Summary of dimensions, material properties, loading conditions and ultimate loads for corrugated carbon steel (CS) web girders.

Ref.	Spec.	a (mm)	h_w (mm)	t_w (mm)	b_f (mm)	t_f (mm)	f_{yw} (MPa)	f_{yf} (MPa)	s_s (mm)	Loaded fold	P^{EXP} (kN)
[22]	1	1000	1000	2.5	250	10	335	476	5	Paralell	149
	2	1000	1000	2.5	250	10	335	476	5	Inclined	170
	3	1000	1500	2.5	250	10	317	476	5	Paralell	152
	4	1000	1500	2.5	250	10	317	476	50	Paralell	168
	5	1000	2000	2	250	12	280	476	5	Edge	107
	6	1000	2000	2	250	12	280	476	50	Inclined	124
[26]	1	750	376	2	120	10	379	389	146	Paralell	131
	2	750	376	2	120	10	379	389	0	Paralell	82
	3	750	376	2	120	10	379	389	104	Inclined	102
	4	750	376	2	120	10	379	389	0	Inclined	96
	5	750	376	2	120	10	379	389	0	Edge	73
[27]	1	1500	500	6	225	20	373	379	90	Inclined	754.2
	2	1500	500	6	225	20	373	379	200	Inclined	956.5
	3	1875	500	6	225	20	373	379	90	Paralell	764.8
	4	1875	500	6	225	20	373	379	200	Paralell	949.0
	5	1875	500	6	225	30	373	379	200	Paralell	1192.0
	6	1140	500	6	225	30	373	379	200	Inclined	1119.3
	7	1500	500	6	225	20	373	379	200	Paralell	1077.7
	8	1500	500	6	225	20	373	379	300	Inclined	1263.9
	9	1875	500	6	225	20	373	379	300	Paralell	1281.0
	10	1500	500	6	225	20	373	379	90	Edge	772.4
[29]	A1	3000	578	3	160	12	375	406	50	Inclined	219
	A2	3000	578	3	160	12	375	406	50	Edge	217
	A3	3000	578	3	160	12	375	406	50	Paralell	181
	B1	3000	578	3	160	12	375	406	50	Paralell	188
	B2	3000	578	3	160	12	375	406	50	Edge	213
	B3	3000	578	3	160	12	375	406	50	Inclined	218

Table 6
Dimensions of the corrugated profiles for carbon steel girders.

Ref.	a_1 (mm)	a_2 (mm)	a_3 (mm)	α (°)	s (mm)	w (mm)
[22]	140	70.7	50	45	210.7	190
[26]	130	150	101	40	280	115
[27]	210	212	145	39	422	375
[29]	140	70.7	50	45	210.7	190

[22] show a reduction in the ultimate loads when the global web ratio increases.

Fig. 19c shows that all the tested girders reported in Table 6 have a similar ratio s/w. It is observed that SS corrugated webs achieved higher ultimate loads for a given value of the ratio s/w compared to CC corrugated webs. As mentioned in Section 2.1, the ratio s/w represents the length of the plate used to produce the corrugated web per unit length along the girder. The influence of the local fold ratio (a_i/t_w) is illustrated in Fig. 19d, in general, girders with higher local fold ratios have lower ultimate loads. According to Kövesdi et al. [27], for $a_i/t_w = 50$ the failures mechanism of carbon steel webs was characterized by global web buckling. For the SS girders the corresponding ratios were $a_i/t_w = 28.3$ for girders SSCWE100, SSCWW300 and SSCWI100, and $a_i/t_w = 29.1$ for girder SSCWP100. Despite this, the failure modes exhibit local web buckling for these girders as seen in Fig. 12. Summing up, for all cases reported in Table 5, the performance of the SS corrugated web girders is better than for CS girders.

Finally, Figs. 20 and 21 show a comparison between the experimental ultimate loads and the predicted resistances obtained considering the contribution of web and flanges —Eq. (1)–, and considering only the contribution of the web –Eq. (3)–. This comparison is performed using the ratio between the fold length a_i and its limiting value according to Eq. (7). As indicated in Eq. (7), the fold length a_i should fulfill Eq. (7) in order to use Eqs. (1) and (2). It is worth noticing in Fig. 20 that Eq. (1) may lead to an overestimation of the patch loading resistance of CS corrugated web girders, but for SS corrugated girders a very good agreement is achieved between predicted resistances and their corresponding experimental values. In contrast, Fig. 21 shows that Eq. (3), neglecting the contribution of the flanges, leads to a significant overestimation of the patch loading resistance of both corrugated CS and SS web girders.

6. Conclusions

In this paper, an experimental investigation on the structural response of stainless steel trapezoidal corrugated web girders subjected to patch loading was conducted. The influence of the loading length, load position, and local fold ratio on the ultimate load behavior was investigated. In all cases analyzed, the girders failed due to local web buckling in the folds beneath the load. For a given length, a complex interaction between the load location in the folds (edge, parallel, and inclined), the flange outstands and the ultimate load was observed, further studies are required to establish this relationship. It was found that the ultimate loads increased almost linearly with the effective loading length.

A numerical model was developed using the finite element method through GMNIA. The model was validated using the load-displacement responses and failure modes obtained experimentally. Moreover, the out-of-plane displacements obtained using a DIC system were compared with numerical results, and a good agreement was attained. In some cases, the numerical results exhibited a stiffer response than the experimental ones. Stress distributions plots indicated that over large areas of the corrugated webs the stresses reached values that ranged between the measured yield stress and the ultimate stress of the material. It provides a clear idea of the utilization of the strain hardening capacity of stainless steel.

A comparison between ultimate loads obtained experimentally and predicted resistances using methodologies available in the literature for carbon steel corrugated web girders (ignoring the strain hardening capacity of stainless steel) showed a good correlation when the contributions of the flange and web were considered. When the contribution of the flange was neglected, the predicted resistances significantly underestimated the test values. A comparison between experimental ultimate loads for stainless steel and carbon steel corrugated webs subjected to patch load showed that the former outperform the latter within the geometric ranges analyzed herein. Despite the good correlation between test loads and predicted resistance, further analyses are required to

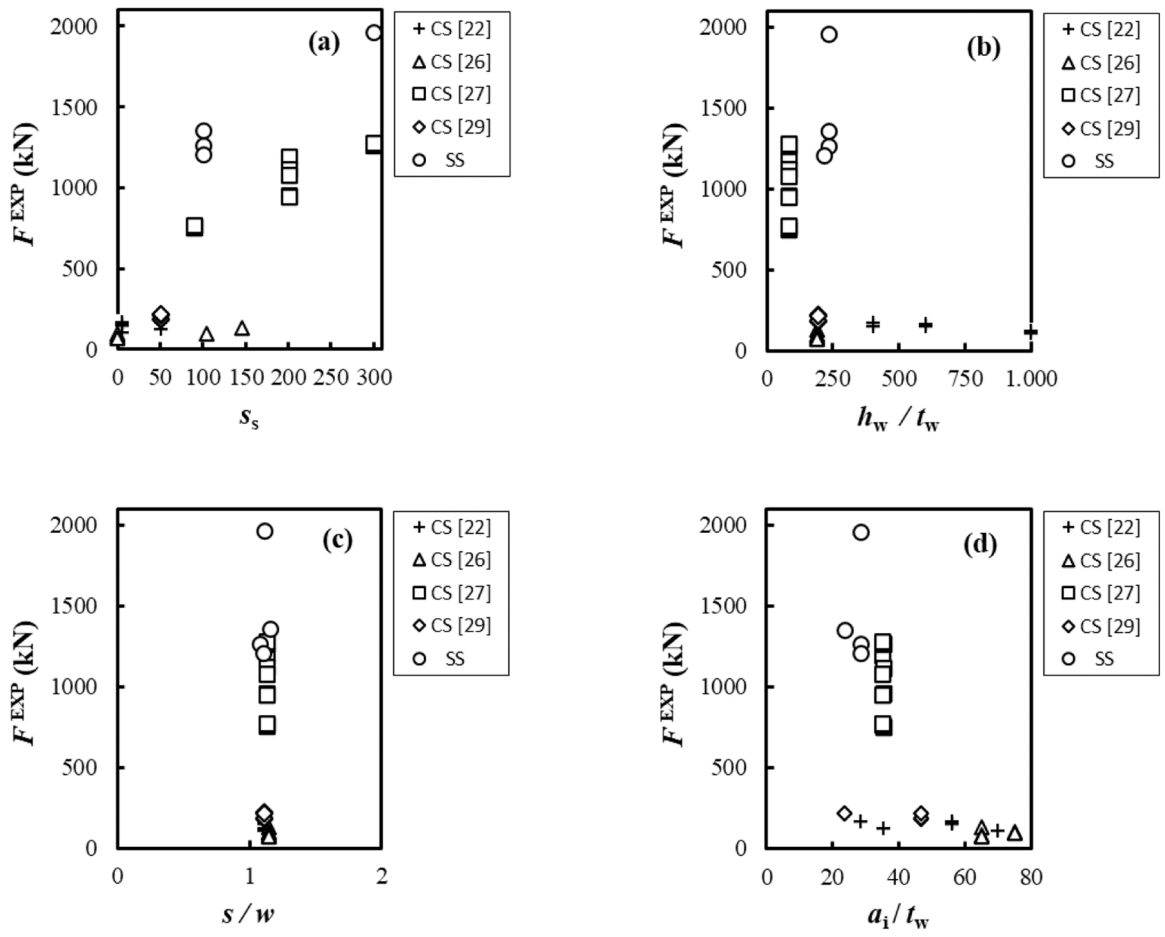

Fig. 19. Influence of various geometric parameters on the experimental ultimate loads F^{EXP} for corrugated CS web girders and corrugated SS web girders.

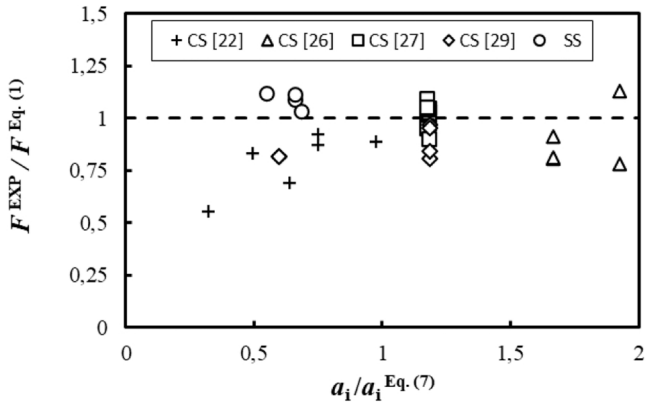

Fig. 20. Comparison between experimental ultimate loads and predicted values using Eq. (1) for corrugated CS and SS web girders.

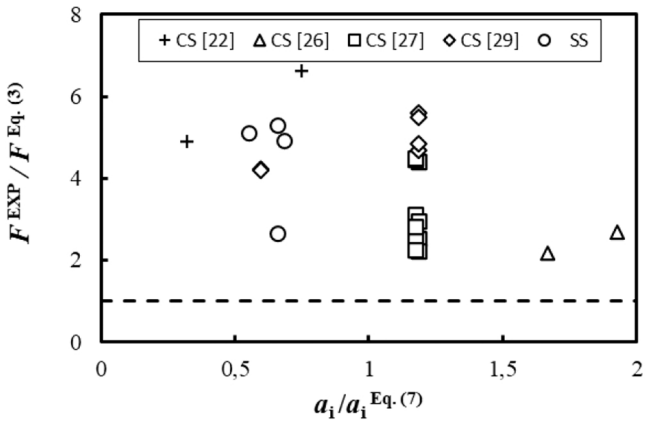

Fig. 21. Comparison between experimental ultimate loads and predicted values using Eq. (3) for corrugated CS and SS web girders.

propose a methodology to obtain the patch loading resistance of stainless steel corrugated web girders considering the strain-hardening characteristics of the material.

In future research, an extensive parametric study is required to extend the range of the geometric parameters evaluated herein. It is necessary to investigate the effects of the flange size, patch loading length, local fold ratios, size of the corrugation profile, and various material plasticity model on the structural response of stainless steel corrugated web girders subject to patch loading.

CRediT authorship contribution statement

Graciano Carlos: Writing – review & editing, Writing – original draft, Visualization, Validation, Supervision, Software, Methodology, Investigation, Formal analysis, Conceptualization. **Flansbjer Mathias:** Writing – original draft, Visualization, Supervision, Resources, Methodology, Investigation, Formal analysis, Data curation, Conceptualization. **Al-Emrani Mohammad:** Writing – review & editing, Writing – original draft, Supervision, Project administration, Methodology, Investigation, Formal analysis, Conceptualization. **Amani Mozhdeh:**

Writing – review & editing, Visualization, Validation, Supervision, Methodology, Investigation, Formal analysis, Data curation. **Casanova Euro:** Writing – review & editing, Visualization, Validation, Software, Methodology, Investigation, Formal analysis.

Declaration of Competing Interest

The authors declare that they have no known competing financial interests or personal relationships that could have appeared to influence the work reported in this paper.

Data Availability

Data will be made available on request.

References

[1] Baddoo NR. Stainless steel in construction: a review of research, applications, challenges and opportunities. J Constr Steel Res 2008;64(11):1199–206. https://doi.org/10.1016/j.jcsr.2008.07.011.

[2] Gardner L. Stability and design of stainless steel structures–review and outlook. Thin-Walled Struct 2019;141:208–16. https://doi.org/10.1016/j.tws.2019.04.019.

[3] Rossi B. Discussion on the use of stainless steel in constructions in view of sustainability. Thin-Walled Struct 2014;83:182–9. https://doi.org/10.1016/j.tws.2014.01.021.

[4] prEN 1993-1-4 Eurocode 3: Design of Steel Structures – Part 1-4: General Rules – Supplementary rules for stainless steels CEN. European Committee for Standardization, Brussels (2023).

[5] ANSI/AISC 370-21, Specification for stainless steel buildings, Chicago, IL, USA: AISC, 2021.

[6] CEN. FprEN 1993-1-5. Eurocode 3: Design of steel structures – Part 1-5: Plated structural elements. Brussels, Belgium: European Committee for Standardization; 2022.

[7] ANSI/AISC 360-16. Specification for structural steel buildings. Chicago, IL, USA: AISC, 2016.

[8] Afshan S, Gardner L. The continuous strength method for structural stainless steel design. Thin-Walled Struct 2013;68:42–9. https://doi.org/10.1016/j.tws.2013.02.011.

[9] Ahmed S, Ashraf M, Anwar-Us-Saadat M. The continuous strength method for slender stainless steel cross-sections. Thin-Walled Struct 2016;107:362–76. https://doi.org/10.1016/j.tws.2016.06.023.

[10] Zhao O, Afshan S, Gardner L. Structural response and continuous strength method design of slender stainless steel cross-sections. Eng Struct 2017;140:14–25. https://doi.org/10.1016/j.engstruct.2017.02.044.

[11] Unosson E. Licentiate thesis, division of steel Structures, Luleå University of Technology. Patch Load Stainl Steel girders: Exp Finite Anal 2003.

[12] Unosson E, Olsson A. Stainless steel girders: resistance to concentrated loads and shear. In: Stainless steel in structures: International experts seminar 20th May 2003. Ascot, UK: Proceedings; 2003. p. 123–30.

[13] E. Unosson, A. Olsson, O. Lagerqvist, A numerical study of the resistance of stainless steel girders subjected to concentrated forces. In Proc. Nordic Steel Const Conf 18-20th June 2001 Finland, Helsinki, 2001, p. 799–806.

[14] dos Santos GB, Gardner L, Kucukler M. Experimental and numerical study of stainless steel I-sections under concentrated internal one-flange and internal two-flange loading. Eng Struct 2018;175:355–70. https://doi.org/10.1016/j.engstruct.2018.08.015.

[15] Graciano C, Loaiza N, Casanova E. Resistance of slender austenitic stainless steel I-girders subjected to patch loading. Structures 2019;20:924–34. https://doi.org/10.1016/j.istruc.2019.07.008.

[16] dos Santos GB, Gardner L. Design recommendations for stainless steel I-sections under concentrated transverse loading. Eng Struct 2020;204:109810. https://doi.org/10.1016/j.engstruct.2019.109810.

[17] Graciano C, Kurtoglu AE, Casanova E. Machine learning approach for predicting the patch load resistance of slender austenitic stainless steel girders. Structures 2021;30:198–205. https://doi.org/10.1016/j.istruc.2021.01.012.

[18] Walport F, Gardner L, Real E, Arrayago I, Nethercot DA. Effects of material nonlinearity on the global analysis and stability of stainless steel frames. J Const Steel Res 2019;152:173–82. https://doi.org/10.1016/j.jcsr.2018.04.019.

[19] Arrayago I, González-de-León I, Real E, Mirambell E. Tests on stainless steel frames. Part I: Preliminary tests and experimental set-up. Thin-Walled Struct 2020;157:107005. https://doi.org/10.1016/j.tws.2020.107005.

[20] Arrayago I, González-de-León I, Real E, Mirambell E. Tests on stainless steel frames. Part II: Results and analysis. Thin-Walled Struct 2020;157:107006. https://doi.org/10.1016/j.tws.2020.107006.

[21] Arrayago I, Rasmussen KJ, Real E. Statistical analysis of the material, geometrical and imperfection characteristics of structural stainless steels and members. J Const Steel Res 2020;175:106378. https://doi.org/10.1016/j.jcsr.2020.106378.

[22] Leiva-Aravena L, Edlund B. Buckling of trapezoidally corrugated webs. Colloquium on Stability of Plate and Shell Structures. Ghent University: ECCS; 1987. p. 107–16.

[23] Kähönen A. Zur Einleitung von Einzellasten in I-Träger mit trapezförmig profilierten Stegen. Stahlbau 1988;57(8):250–2 ([In German]).

[24] Luo R, Edlund- B. Ultimate strength of girders with trapezoidally corrugated webs under patch loading. Thin-Walled Struct 1996;24(2):135–56. https://doi.org/10.1016/0263-8231(95)00029-1.

[25] Elgaaly M, Seshadri A. Girders with corrugated webs under partial compressive edge loading. J Struct Eng ASCE 1997;123(6):783–91. https://doi.org/10.1061/(ASCE)0733-9445(1997)123:6(783).

[26] Elgaaly M, Seshadri A. Depicting the behavior of girders with corrugated webs up to failure using non-linear finite element analysis. Adv Eng Softw 1998;29(3-6):195–208. https://doi.org/10.1016/S0965-9978(98)00020-9.

[27] Kövesdi B, Braun B, Kuhlmann U, Dunai L. Patch loading resistance of girders with corrugated webs. J Constr Steel Res 2010;66(12):1445–54. https://doi.org/10.1016/j.jcsr.2010.05.011.

[28] Kövesdi B, Dunai L. Determination of the patch loading resistance of girders with corrugated webs using nonlinear finite element analysis. Comput Struct 2011;89(21-22):2010–9. https://doi.org/10.1016/j.compstruc.2011.05.014.

[29] Ljungström N, Karlberg O. Master thesis, Department of Architecture and Civil Engineering, Chalmers University of Technology. Girders Trapez Corrugat webs patch Load 2011.

[30] M. Al-Emrani, B. Edlund, R. Haghani. Girders with trapezoidally corrugated webs-under patch loading. In Proc. of the Nordic Steel Const Conf 5-7th September 2012, Oslo, Norway, 2012, p. 107–116.

[31] Inaam Q, Upadhyay A. Behavior of corrugated steel I-girder webs subjected to patch loading: Parametric study. J Constr Steel Res 2020;165:105896. https://doi.org/10.1016/j.jcsr.2019.105896.

[32] Maiorana E, Poh'sié GH, Emechebe CC. Non-linear analysis of corrugated plate girders under patch loading. Int J Steel Struc 2023;23(1):1–9. https://doi.org/10.1007/s13296-023-00726-2.

[33] Kumar SA, Sofi FA, Bhat JA. Estimation of patch-loading resistance of steel girders with unequal trapezoidal web-corrugation folds using nonlinear FE models and artificial neural networks. Structures 2023;48:1651–69. https://doi.org/10.1016/j.istruc.2023.01.049.

[34] Kumar SA, Sofi FA, Bhat JA, Zhou M. Comprehensive analysis of corrugated-web steel girders: A systematic review. Thin-Walled Struct 2025;208:112636. https://doi.org/10.1016/j.tws.2024.112636.

[35] D. Sæmundsson, S. Ingólfsdóttir Nonlinear finite element analysis of stainless steel corrugated web girders subjected to patch loading. Master thesis, Department of Architecture and Civil Engineering, Chalmers University of Technology, 2021.

[36] Pasternak H, Branka P. Tragverhalten von Wellstegträgern unter lokaler Lasteinleitung. Bauingenieur 1999;74:219–24 (In German).

[37] Nikoomanesh MR, Goudarzi MA. Patch loading capacity for sinusoidal corrugated web girders. Thin-Walled Struct 2021;169:108445. https://doi.org/10.1016/j.tws.2021.108445.

[38] EN ISO 6892-1, Metallic Materials–Tensile. Test, Part 1: Method Test room Temp 2011.

[39] Amani M, Al-Emrani M, Flansbjer M. Shear behavior of stainless steel girders with corrugated webs. J Const Steel Res 2023;210:108086. https://doi.org/10.1016/j.jcsr.2023.108086.

[40] Aramis User Manual – Software, GOM mbH, Braunshweig Germany 2009.

[41] Ansys® Academic Research Mechanical, Release 2024 R1, Help System, Ansys Parametric Design Language Guide, ANSYS, Inc.

[42] CEN. FprEN 1993-1-14. Eurocode 3: Design of steel structures – Part 1-14. Design assisted by finite element analysis. Brussels, Belgium: European Committee for Standardization; 2022.

[43] Roberts TM, Rockey KC. A mechanism solution for predicting the collapse loads of slender plate girders when subjected to in-plate patch loading. Proc Inst Civ Eng 1979;67(2):155–75.